ARTICLE

Effect of High Temperature Curing on the Frost Resistance of Recycled Aggregate Concrete and the Physical Properties of Second-Generation Recycled Coarse Aggregate under Freeze-Thaw Cycles

Xintong Chen, Pinghua Zhu[*], Xiancui Yan, Lei Yang and Huayu Wang

Changzhou City Key Laboratory of Building Energy-Saving Technology, Department of Civil Engineering, Changzhou University, Changzhou, 213164, China

[*]Corresponding Author: Pinghua Zhu. Email: zph@cczu.edu.cn

ABSTRACT

With the emphasis on environmental issues, the recycling of waste concrete, even recycled concrete, has become a hot spot in the field of architecture. But the repeated recycling of waste concrete used in harsh environments is still a complex problem. This paper discusses the durability and recyclability of recycled aggregate concrete (RAC) as a prefabricated material in the harsh environment, the effect of high-temperature curing (60°C, 80°C, and 100°C) on the frost resistance of RAC and physical properties of the second generation recycled coarse aggregate (RCA$_2$) of RAC after 300 freeze-thaw cycles were studied. The frost resistance of RAC was characterized by compressive strength, relative dynamic elastic modulus, and mass loss. As the physical properties of RCA$_2$, the apparent density, water absorption, and crushing value were measured. And the SEM images of RAC after 300 freeze-thaw cycles were shown. The results indicated that the frost resistance of RAC cured at 80°C for 7 days was comparable to that cured in the standard condition (cured for 28 days at 20°C ± 2°C and 95% humidity), and the RAC cured at 100°C was slightly worse. However, the frost resistance of RAC cured at 60°C deteriorated seriously. The RAC cured at 80°C for 7 days is the best. Whether after the freeze-thaw cycle or not, the RCA that curd at 60°C, 80°C, and 100°C for 7 days can also meet the requirements of Grade III RCA and be used as the aggregate of non-bearing part of prefabricated concrete components. RCA$_2$ which is cured at 80°C for 7 days had the best physical properties.

KEYWORDS

Freeze-thaw cycles; curing condition; recycled aggregate concrete; second-generation recycled coarse aggregate

1 Introduction

In recent years, the rapid development of urbanization in China has led to the construction of a large number of buildings and infrastructure, which has consumed many natural resources [1]. In addition, these buildings will be demolished after reaching the designed service life, thus producing construction waste. In order to reduce the consumption of aggregate natural resources and construction waste, recycled aggregate concrete (RAC) has attracted many scholars' attention [2]. RAC is a new type of green concrete, which is made of recycled coarse aggregate instead of natural coarse aggregate (RCA) according to a certain proportion. Besides, for the multi-generation sustainable development of concrete,

the RAC could also be crushed to obtain the second-generation recycled coarse aggregate (RCA_2) and the multi-generation RAC [3–6]. The physical properties of RCA_2 play a decisive role in the mechanical and durability performance of multi-generation RAC [7–11]. Therefore, research on the serviceability in harsh environments of RAC and the physical properties of RCA_2 is needed for the extensive application of RAC.

The production efficiency of precast concrete components needs to be increased with the ongoing growth of prefabricated buildings [12–14]. Traditional concrete preparation necessitates a normal 28-day curing period, which not only slows down the building but also uses up a lot of time, materials, and money. Numerous studies have been conducted, mostly by raising the temperature of the curing process in order to reduce the curing time and increase the early strength of concrete [15–19]. Shumuye et al. [20] found that concrete cured at high temperatures for 7 days has more hydration products than standard curing concrete. According to Xu et al. [21], binders containing fly ash have a more temperature-sensitive hydration process when compared to binders with ground granulated blast furnace slag. According to Shi et al. [22], steam-cured concrete's mechanical characteristics declined with an increase in curing temperature, while its brittleness rose. Algourdin et al. [23] discovered that when the temperature rises, RAC's residual compressive strength and elastic modulus decline as its porosity rises. The relationship between thermal conductivity, porosity, and most likely pore size was researched by Chen et al. [24]. They discovered that the curing temperature significantly influences the degree of hydration and regulates the development of thermal conductivity. The chloride ion transport coefficient was shown to decrease with increased curing time by Du et al. [25]. Erdem et al. [26] concluded that when the steam curing time was extended from 5 to 10 h, the compressive strengths reached 30.2 and 34.1 MPa at the highest steam curing temperature of 80°C. Kjellsen [27] reported that low-temperature curing of concrete was unfavorable to developing early strength. According to Sajedi's [28] research, raising the curing temperature was good for strength increases of 3–7 days but bad for those of 28–90 days. One of the most efficient ways to encourage the pozzolanic reaction between supplemental cementitious material and $Ca(OH)_2$ is to raise the temperature. $Ca(OH)_2$ concentration and the quantity of active molecules can both be raised by increasing cement hydration [29]. Under 80°C, the C-S-H gel in ordinary concrete and RAC became more porous than it was at 20°C [30]. However, little study has been done on how short-term high-temperature curing affects the mechanical properties and durability of RAC, and the physical characteristics of RCA_2. How to shorten the preparation time of RAC and the RCA_2 that meet the requirements is an urgent problem to be solved.

Frost resistance is one of the most essential durability of concrete, and the freeze-thaw cycles will cause damage to concrete [31–33]. When the replacement ratio of RCA was low, Huda et al. [34] noted that there was minimal difference between the frost resistance of RAC and natural aggregate concrete. According to Liu et al. [35], RAC made by RCA from parent concrete with a high strength has superior frost resistance than parent concrete with a low strength. According to Xiao et al. [36], under the circumstance of a 100% replacement ratio of RCA, the rapid accumulation of freeze-thaw damage had a substantial impact on the service life of RAC. According to Wang et al. [37], the useful addition of glazed hollow beads can considerably increase the frost resistance of RAC while offsetting the negative impacts of RCA. According to Liu et al. [38], denitrifying bacteria inserted in the open pores of RAC induced a decrease in water absorption of 33.0%, preventing the absorption of external water and reducing the expansion brought on by water freezing. In the 3% Na_2SO_4 solution, Xiao et al. [39] found that the deterioration degree of RAC was less than that of water in the initial stage of the freeze-thaw cycle. After 200 freeze-thaw cycles, the deterioration degree of recycled concrete was greater than that of water. Wei et al. [40] found that adhesive mortar and interfacial transition zone (ITZ) are the primary carriers of freeze-thaw damage transfer. However, it is unclear whether the RCA_2 obtained by crushing RAC served in a freeze-thaw environment can be used, especially the RAC exposed to high-temperature curing for short periods.

This research can significantly improve the sustainable utilization capacity of RAC prefabricated components.

To compare the impacts of different curing regimes on RAC and RCA_2. In this study, the impacts of high-temperature curing (60°C, 80°C, and 100°C) for 7 days on the frost resistance of RAC and the physical properties of the RCA_2 in the freeze-thaw environment were explored. From the perspectives of compressive strength, relative dynamic elastic modulus, and mass loss, the frost resistance of RAC was assessed. The RCA_2's physical characteristics were evaluated in terms of apparent density, water absorption, and crushing value. In addition, the morphology of RAC cured at high temperature for 7 days was observed by the scanning electron microscope (SEM). This study tries to find a curing method for RAC that can be used sustainably to shorten the curing time and make it sustainable in a freeze-thaw environment.

2 Materials and Methods

2.1 Materials and Mix Proportions

P·O 42.5 ordinary Portland cement, fly ash (Grade II), and silica fume were used as the cementitious materials, with apparent densities of 2829 and 2759 kg/m^3, respectively. Natural river sand with the apparent density of 2620 kg/m^3 and the fineness modulus of 2.4 was used as the fine aggregate. RCA, with a particle size range of 4.75–20 mm, was produced by Changzhou Wujin Lvhe Co., Ltd. (China). The physical properties of RCA are shown in Table 1, meeting the requirements of Grade II RCA in Chinese standard GB/T 25177-2010 [41]. The replacement rate of RCA to natural coarse aggregate was 100%. The polycarboxylic acid with water-reducing efficiency of 20% and Clariant AE-2 air entraining agent was used as the chemical admixtures. The target design strength of RAC was C50, and the target slump was 150–200 mm. The mixed proportion of RAC is shown in Table 2.

Table 1: The physical properties of RCA

Apparent density	Bulk density	Adhesion mortar content	Water absorption	Crushing value
2545 kg/m^3	1445 kg/m^3	37.9%	4.7%	16.7%

Table 2: The mix proportion of RAC (kg/m^3)

RCA	Sand	Cement	Fly ash	Silica fume	Water	Water reducer	Air-entraining agent
1012	662	403	81	54	177	2.69	0.16

2.2 Sample Preparation

The prismatic samples with dimensions of 100 mm × 100 mm × 100 mm and 100 mm × 100 mm × 400 mm were made. After casting, the samples were exposed to different high-temperature curing (60°C, 80°C, and 100°C) for 7 days. For comparison, the samples were cured at a standard curing room (20°C ± 2°C and RH > 95%) for 28 days as the control group. The experimental process of this study is shown in Fig. 1.

2.3 Test Methods

2.3.1 The Frost Resistance of RAC

The RAC was submerged in a water-filled rubber sleeve after curing. At least 5 mm should separate the sample's aqueous surface from that of the sleeve. It was then put in a TDR-3F48 Concrete Freeze-Thaw Test Chamber to undergo freeze-thaw cycles. The frost resistance of RAC was tested according to the rapid

freeze-thaw experimental methods in GB/T 50082-2009 [42]. Freeze-thaw process 50 times takes about 7 to 8 days. To simulate the stress state of RAC under actual conditions, the ultimate tensile stress of 0.3 was applied to the sample before the freeze-thaw cycles. Precisely, the sample was placed on the pressure testing machine, and cyclic tensile strain was used 10 times before each test cycle [43,44]. A total of 300 freeze-thaw cycles were performed on the RAC. To evaluate the frost resistance of RAC, compressive strength, relative dynamic elastic modulus, and mass loss were used.
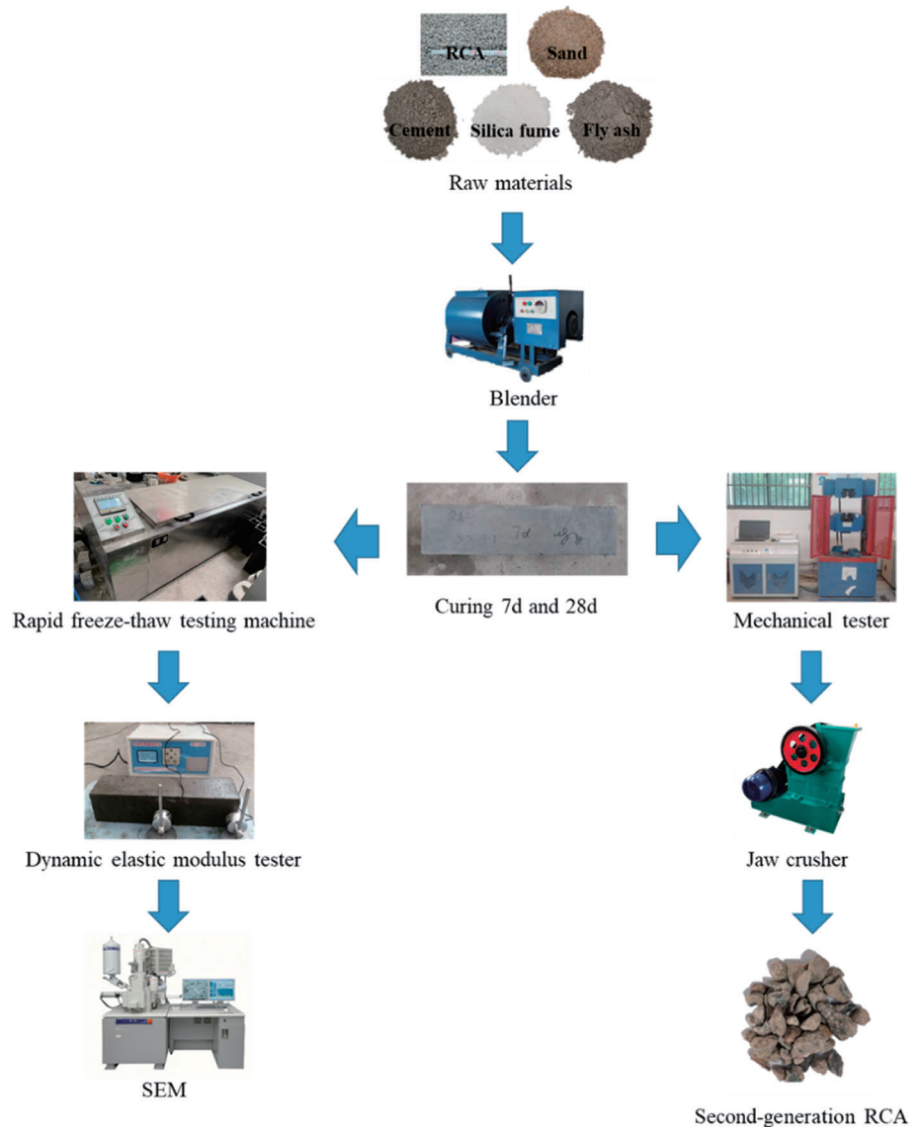

Figure 1: Experimental process chart

After every 100 freeze-thaw cycles, the compressive strength of RAC (100 mm × 100 mm × 100 mm) was tested using a TYW-2000 microcomputer control electro-hydraulic servo universal testing equipment.

The transverse fundamental frequency of RAC was measured every 50 freeze-thaw cycles.

According to GB/T 50082-2009 [42], the relative dynamic elastic modulus shall be calculated according to formula (1).

$$p = \frac{f_n}{f_0} \times 100 \tag{1}$$

where p is the relative dynamic elastic modulus of RAC after n freeze-thaw cycles (%); f_n is the transverse fundamental frequency (Hz) of RAC after n freeze-thaw cycles; f_0 is the initial transverse fundamental frequency before freeze-thaw cycles (Hz).

The mass of the samples (100 mm × 100 mm × 400 mm) was measured every 50 freeze-thaw cycles. According to GB/T 50082-2009 [42]. The mass loss of the sample was calculated according to formula (2)

$$\Delta W_n = \frac{W_0 - W_n}{W_0} \times 100 \tag{2}$$

where ΔW_n is the mass loss (%) of RAC after n freeze-thaw cycles; W_0 is the mass of RAC before freeze-thaw cycles (g); W_n is the mass of RAC after n freeze-thaw cycles (g).

2.3.2 The Physical Properties of RCA₂

After 300 freeze-thaw cycles, the RAC was crushed by a jaw crusher, and the particle size of RCA$_2$ of 5–20 mm was screened. Then, RCA$_2$ was washed to remove excess impurities and dried in a 60°C ± 2°C oven for 12 h. Besides, the RAC without freeze-thaw cycles (after curing) was also crushed to produce the RCA$_2$ for comparison. According to the specifications of GB/T 25177-2010 [41] and GB/T 14685-2011 [45], the apparent density, water absorption, and crushing value of RCA$_2$ were evaluated.

Because the particle size of the RCA$_2$ was less than 37.5 mm, the apparent density was measured by the wide-mouth bottle method. Test method of curing value: Placed circular mold with RCA under mechanical tester. Evenly load to 200 kN at the speed of 1 kN/s and then unload after 5 s of stability. Poured out the sample from the circular mold and sieved out the crushed fine particles with a sieve with a hole diameter of 2.36 mm. Water absorption of the RCA$_2$ was calculated according to formula (3). The curing value of the RCA$_2$ was calculated according to formula (4).

$$W = \frac{G_1 - G_2}{G_2} \times 100 \tag{3}$$

where W is the water absorption (%) of the RCA$_2$; G_1 is the mass of the RCA$_2$ with saturated surface dry condition (g); G_2 is the mass of the RCA$_2$ with drying regime (g).

$$Q_e = \frac{G_1 - G_2}{G_1} \times 100 \tag{4}$$

where Q_e is the curing value of the RCA$_2$; G_1 is the mass of the RCA sample (g); G_2 is the sample mass of sieve residue after the crushing test (g).

2.3.3 SEM

SEM (JSM-IT 100) was used to observe the micromorphology of the second-generation RAC. RAC portions of 8 mm × 8 mm × 5 mm were prepared by diamond saw. To avoid contaminating the lens, the pieces' surface was cleaned with compressed gas. The sections were then submerged in an ethanol solution for seven days before being dried at 60°C for twenty-four hours. These portions were sprayed with gold before the measurement.

3 Results and Discussion

3.1 The Frost Resistance of RAC

3.1.1 Compressive Strength

Fig. 2 shows the effects of curing regimes on the compressive strength of RAC after freeze-thaw cycles. It can be shown that the compressive strength of RAC cured at 100°C for 7 days was about the same as that at conventional curing for 28 days for the RAC without freeze-thaw cycles (after curing). The compressive strength of RAC was 20.5% and 6.4% less than that of conventional curing for 28 days when it was cured at 60°C and 80°C for 7 days, respectively. Early RAC strength increases in terms of compressive strength benefited by high-temperature curing.
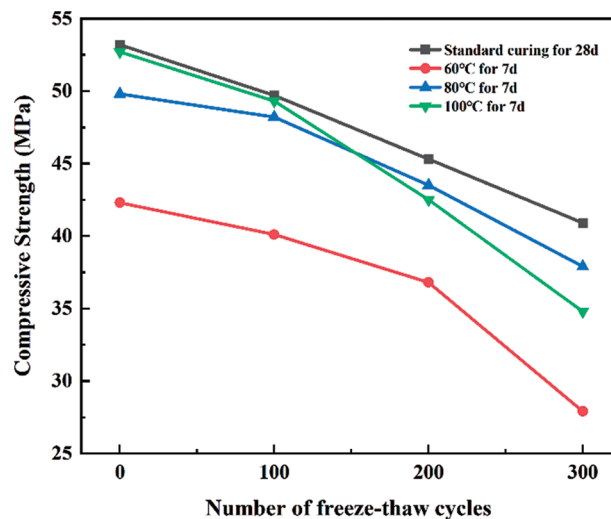

Figure 2: Effects of curing regimes on the compressive strength of RAC after freeze-thaw cycles

The compressive strength of RAC decreased as the number of freeze-thaw cycles increased. After 300 freeze-thaw cycles, the compressive strength of RAC at 28 days of standard curing was reduced by 23.1%. After 300 freeze-thaw cycles, the compressive strength of RAC that was cured at 60°C, 80°C, and 100°C for 7 days fell by 34.0%, 24.5%, and 33.9%, respectively. It is interesting to note that after 100 freeze-thaw cycles, the compressive strength of RAC treated at 100°C was 2.28% higher than that cured at 80°C for 7 days. However, when the number of freeze-thaw cycles was 200 times, the compressive strength of the RAC cured at 80°C was 2.35% higher than that of the RAC cured at 100°C for 7 days. The primary causes of the negative impacts on the long-term performance of concrete from curing at high temperatures are uneven distribution of hydration products and dense water crust [46,47]. When the curing temperature is too high, this situation may be aggravated. Uneven distribution of hydration products led to bad internal pores in RAC. This is why the compressive strength of RAC cured at 100°C decreased more rapidly than RAC cured at 80°C after 100 freeze-thaw cycles. The performance of RAC cured at 80°C for 7 days was better than that cured at 60°C and 100°C after freeze-thaw cycles. For 7 days of 60°C high-temperature curing, the compressive strength of RAC cannot meet the requirements of frost resistance due to the short curing periods. For 7 days of 100°C high-temperature curing, the hydration products formed quickly and had no time to even distribution, decreasing the compactness and frost resistance of RAC.

3.1.2 Relative Dynamic Elastic Modulus

The effects of different curing regimes on the relative dynamic elastic modulus of RAC following freeze-thaw cycles are depicted in Fig. 3. The relative dynamic elastic modulus of RAC treated at 80°C and 100°C for 7 days was practically the same as that at conventional curing for 28 days when the number of freeze-thaw cycles was no more than 200. The RAC cured at 80°C and 100°C for 7 days could be used in a slight freeze-thaw environment. However, for 300 freeze-thaw cycles, the relative dynamic elastic modulus of RAC cured at 80°C and 100°C for 7 days decreased to 23.5% and 27.0%, respectively, larger than that at standard curing for 28 days (22.5%). The relative dynamic elastic modulus of RAC cured at 60°C for 7 days is the lowest, reaching 67.5% after 300 freeze-thaw cycles. Curing at 60°C for 7 days was not appropriate for the RAC in a freeze-thaw environment.
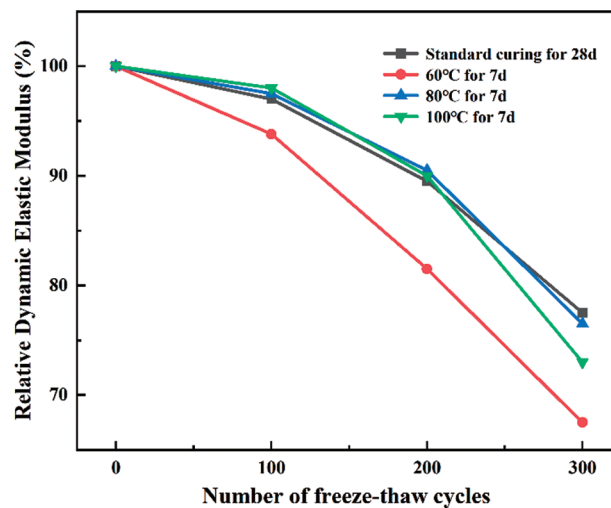

Figure 3: Effects of curing regimes on the relative dynamic elastic modulus of RAC after freeze-thaw cycles

The RAC cured at 60°C for 7 days did not have adequate curing temperature and time. This kind of curing regime had less hydration of cement. The internal pores and micro-cracks of RAC before freeze-thaw cycles couldn't be filled better by hydration products. The RAC cured at 60°C for 7 days had a lot of undesirable pores. Undesirable pores and uneven distribution of hydration products might lead to stress concentration. Under freeze-thaw cycles, the RAC might suffer more internal damage. The uniformity of hydration product distribution and the extent of undesirable pores affected internal damage. Relative dynamic elastic modulus could reflect the extent of internal damage of the RAC [48].

The RAC cured at 80°C for 7 days can meet the 100-year design requirement of moderate water saturation in cold regions and the 50-year design requirement of high-water saturation in cold areas [49].

3.1.3 Mass Loss

The effects of curing regimes on the mass loss of RAC following freeze-thaw cycles are depicted in Fig. 4. Fig. 4 illustrates how the mass of RAC rose throughout the course of 100 freeze-thaw cycles. Because RAC has the most internal pores, the mass of the material grew the highest during the initial stages of freeze-thaw cycles after curing at 60°C for 7 days. However, the mass loss of RAC cured at 60°C was also the largest as the number of freeze-thaw cycles increased. RAC cured at 60°C had the lowest ability to resist the development of cracks during freeze-thaw cycles; the gradual increase of cracks led to concrete falling, resulting in the most mass loss. After 300 freeze-thaw cycles, the mass loss of RAC cured at 80°C for 7 days (1.27%) is almost the same as that at standard curing for 28 days (1.24%), which is lower than those cured at 60°C and 100°C (1.6% and 1.51%).
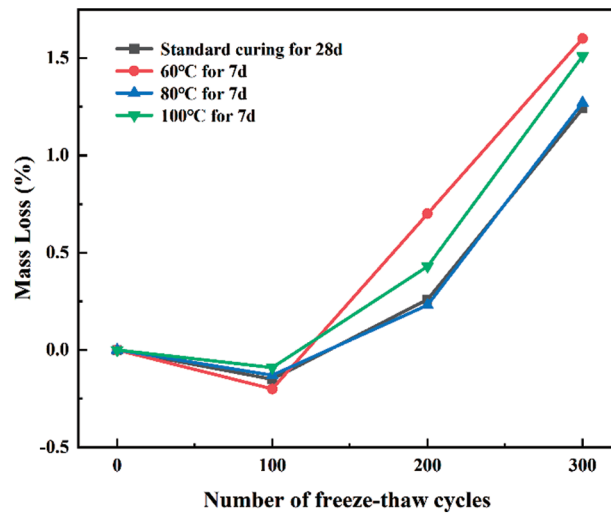
Figure 4: Effects of curing regimes on the mass loss of RAC after freeze-thaw cycles

The primary cause of the mass loss was RAC injury. Water partially fills the pores of the concrete at the start of freeze-thaw cycles [50]. The cracks in the concrete were not severe and partially filled by new hydration products, which might lead to a slight increase in mass. The amount of RAC microcracks keeps growing as a result of more frequent freeze-thaw cycles [40]. Hydrostatic pressure made the surface of the RAC spall. The mass loss of RAC kept rising after 100 freeze-thaw cycles.

3.2 The Physical Properties of RCA_2

3.2.1 Apparent Density

The apparent density of the RCA_2 from the RAC at various curing regimes both before and after 300 freeze-thaw cycles is depicted in Fig. 5. According to Fig. 5, the apparent density of the RCA_2 was typically higher before freeze-thaw cycles than it was after. The apparent density of RCA_2 may have decreased as a result of the freeze-thaw cycles, which also increased the porosity of RAC and damaged its interior.
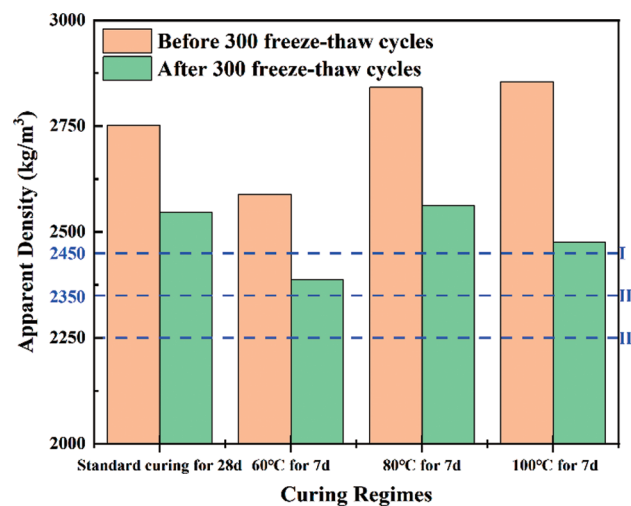

Figure 5: The apparent density of the RCA_2 from the RAC at different curing regimes before and after 300 freeze-thaw cycles

Before freeze-thaw cycles, RCA_2 from RAC cured at 60°C for 7 days had a lower apparent density than RCA_2 from RAC cured at 80°C and 100°C for 7 days, but both of these RAC cures had greater apparent densities than RCA_2 from RAC cured at 60°C for 7 days. High-temperature curing improved the early strength of RAC, and the aggregate was well combined with mortar, which resulted in fewer pores in the RCA_2. After 300 freeze-thaw cycles, the apparent density of the RCA_2 from the RAC cured at 60°C and 100°C was lower than that at standard curing. The RAC cured at too high or too low temperature could decrease the adhesive force between paste and aggregates, which was not conducive to the apparent density of the RCA_2. However, the difference between the apparent density of the RCA_2 from the RAC cured at 80°C for 7 days and cured at standard curing for 28 days was insignificant, indicating that the optimal choice was that RAC cured at 80°C for 7 days.

According to GB/T 25177-2010 [22], China's RCA utilized in structural concrete can be categorized into three categories. The use of RCA is prohibited if its properties fall short of Grade III standards. The limits of the apparent density of RCA with different grades are also shown in Fig. 5. It can be observed in Fig. 5 that the apparent density of RCA from the RAC cured at 80°C and 100°C after 300 freeze-thaw cycles reached the criteria of Grade I, while that from the RAC cured at 60°C reached the requirements of Grade II. The RCA_2 from the RAC with high temperature curing for 7 days served in a freeze-thaw environment performed excellent apparent density.

3.2.2 Crushing Value

Fig. 6 shows the crushing value of the RCA_2 from the RAC at different curing regimes before and after 300 freeze-thaw cycles. It was evident that the crushing value of the RCA_2 from the RAC before 300 freeze-thaw cycles was lower than that after 300 freeze-thaw cycles. SEM micrograph showed that concrete would generate more cracks and pores after freeze-thaw cycles [51]. The RCA_2 from RAC, after 300 freeze-thaw cycles, has more cracks and pores than the RCA_2 without freeze-thaw cycles. Those might generate some damage in the RCA_2. This was due to the freeze-thaw damage inside the RAC, which reduced the ability of RCA_2 to resist external forces.
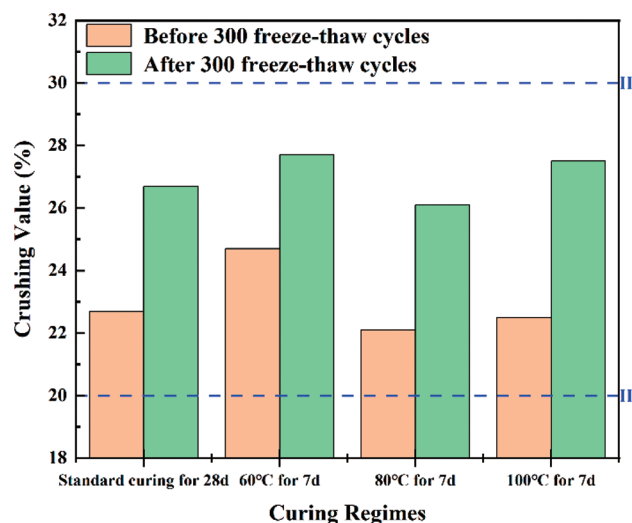

Figure 6: The crushing value of the RCA_2 from the RAC at different curing regimes before and after 300 freeze-thaw cycles

Before freeze-thaw cycles, the crushing value of the RCA_2 from RAC cured at 60°C for 7 days was 8.8% higher than that at standard curing for 28 days. After curing at 80°C and 100°C for 28 days, the crushing

value of RCA_2 decreased by 2.6% and 0.9%, respectively compared with that at standard curing. After 300 freeze-thaw cycles, the crushing value of the RCA_2 from RAC cured at 60°C and 100°C was 3.7% and 3.0% higher than that at standard curing for 28 days. However, the crushing value of the RCA_2 from RAC cured at 80°C was 2.2% lower than that at standard curing for 28 days. The consistent distribution of hydration products and pores results from low curing temperatures. No consistently distributed hydration products and coarser pores are produced at higher temperatures [52]. Low curing temperatures, however, sharply lower the hydration rate and result in a relatively small number of early hydration products and a loose structure [53–55]. This might lead to the crushing value of the RCA_2 being relatively high when curing at 60°C and 100°C. In the case of the crushing value, the RCA_2 from RAC cured at 80°C after freeze-thaw cycles could be more suitable for use.

The limits of the crushing value of RCA with different grades were also shown in Fig. 6. Before and after 300 freeze-thaw cycles, the crushing value of the RCA from the RAC at standard curing for 28 days or high temperature curing for 7 days all met the standards of Grade III. Thus, RCA_2 belonged to Grade III, although the apparent density reached Grade II (Fig. 5).

3.2.3 Water Absorption

The water absorption of the RCA_2 from the RAC at various curing regimes both before and after 300 freeze-thaw cycles is depicted in Fig. 7. As can be observed from Fig. 7, the findings of crushing value were similar in that the RCA_2's water absorption rose greatly after 300 freeze-thaw cycles were applied to the RAC.
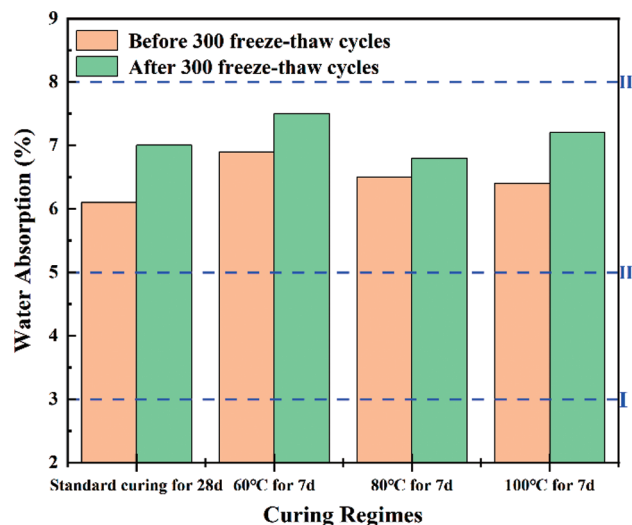

Figure 7: The water absorption of the RCA_2 from the RAC at different curing regimes before and after 300 freeze-thaw cycles

When RAC was at standard curing for 28 days, the water absorption of RCA_2 was at its lowest level prior to freeze-thaw cycles. The water absorption of RCA_2 from RAC cured at 60°C, 80°C, and 100°C for 7 days was 13.1%, 6.6%, and 4.9% higher than that at standard curing for 28 days. The progressive decrease in RCA_2's water absorption was caused by an increase in curing temperature. The reason may be that more hydration products can be produced when RAC was at high-temperature curing, which reduces the water absorption of RCA_2.

After 300 freeze-thaw cycles, the water absorption of RCA_2 from RAC at 60°C and 100°C for 7 days was 7.1% and 2.9% higher than that at standard curing for 28 days, while that from RAC at 80°C for 7 days was 2.9% lower than that at standard curing for 28 days. When RAC was subjected to freeze-thaw cycles, too high or too low a curing temperature could diminish the compactness of RAC and increase internal freeze-thaw damage and cracks, leading to increased water absorption of RCA_2. To shorten the curing periods of RAC by increasing curing temperature, curing at 80°C for 7 days was the optimal choice for the RAC when exposed to freeze-thaw cycles.

Fig. 7 displays the water absorption limits of RCA of various grades. It can be observed that all the RCA_2 from RAC with 7 days of high-temperature curing suffered 300 freeze-thaw cycles and can meet the requirements of Grade III. Although the freeze-thaw damage in RAC increased the water absorption of RCA_2, it can still be used as the aggregate of concrete structures.

3.3 SEM Observation

Fig. 8 shows the SEM micrograph of RAC at different curing regimes after 300 freeze-thaw cycles. After freeze-thaw cycles, no apparent pores occurred in the mortar of RAC at standard curing for 28 days (Fig. 8a). At high-temperature of 80°C for 7 days (Fig. 8c). This might be the reason for the frost resistance of RAC curing at 80°C for 7 days and RAC at standard curing for 28 days having almost the same properties. This might lead to the physical properties of RCA_2 curing at 80°C for 7 days and for 28 days at standard both were excellent, too. After 300 freeze-thaw cycles, there were more pores in RAC with 60°C curing for 7 days (Fig. 8b). After 300 freeze-thaw cycles, there were apparent porous structures in RAC with 100°C curing for 7 days (Fig. 8d), the degree of separation between mortar and aggregate was large, and there were many cracks inside the mortar. This might generate some damage in the RAC and the RCA_2. Internal damage decreased the RAC's ability to resist freezing and the RCA_2's physical characteristics. All curing procedures generated hydration products. ITZ is where C-S-H gel is mainly found. ITZ is the RAC's most vulnerable point in terms of strength and durability loss [56]. Despite the presence of C-S-H gel inside ITZ (Figs. 8a and 8b), it was not enough to withstand the invasion of freeze-thaw damage.
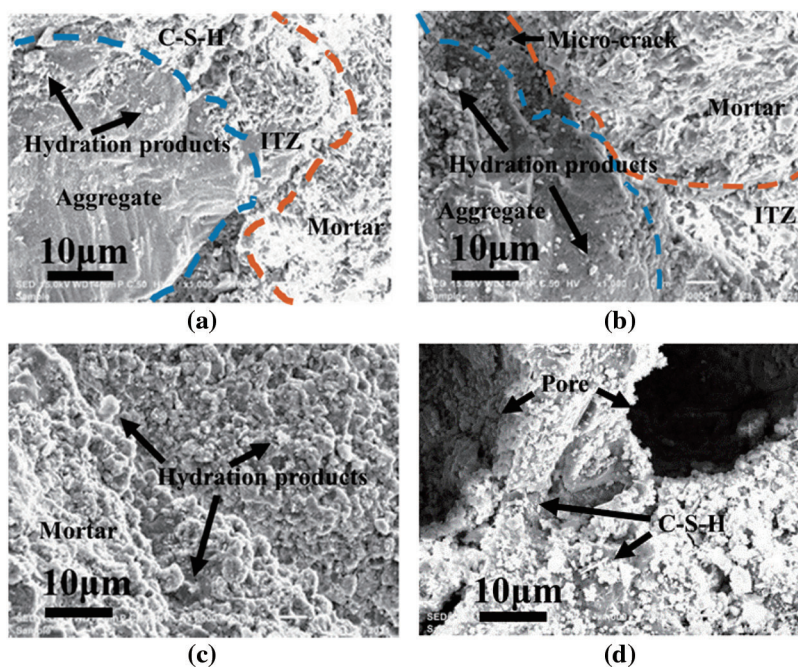

Figure 8: SEM micrograph of RAC at different curing regimes after 300 freeze-thaw cycles: (a) standard curing for 28 days; (b) curing at 60°C for 7 days; (c) curing at 80°C for 7 days; (d) curing at 100°C for 7 days

Conclusion: Curing at a high temperature of 80°C can improve RAC's ability to withstand frost, and temperatures that are too high or too low prevent the development of RAC's strength and durability.

4 Conclusions

The frost resistance of RAC is significantly influenced by high-temperature curing. The frost resistance of RAC that had been cured at 80°C for 7 days was similar to that of RAC that had been cured under the usual condition (20°C ± 2°C and RH > 95%), while the RAC that had been cured at 100°C was only marginally worse. However, the frost resistance of RAC cured at 60°C deteriorated seriously. The RAC cured at 80°C for 7 days can meet the 100-year design requirement of moderate water saturation in cold regions and the 50-year design requirement of high-water saturation in cold areas. After 300 freeze-thaw cycles, SEM results showed apparent pores and cracks in RAC with 7 days of 60°C and 100°C curing, which indicated poor frost resistance.

Although the freeze-thaw damage of RAC resulted in the decrease of apparent density, and the increase of water absorption and crushing value of RCA_2, it can still meet the requirement of Grade III RCA and be used as the aggregate of non-bearing parts of concrete structures. Regarding the physical properties of RCA_2, curing at 80°C for 7 days was the optimal choice for the RAC when exposed to freeze-thaw cycles.

Proper curing temperature can ensure the performance of RAC and save production time effectively. In addition, it is feasible to recycle RAC damaged by freeze-thaw cycles as RCA_2, which will provide favorable support for the reuse of waste-recycled concrete in harsh environments. However, if this kind of aggregate is to be used in load-bearing structures, it is necessary to modify the aggregate and upgrade its quality to at least Grade II.

Conflicts of Interest: The authors declare that they have no conflicts of interest to report regarding the present study.

References

1. Bian, J. W., Zhang, W. B., Shen, Z. Z., Li, S., Chen, Z. L. (2021). Analysis and optimization of mechanical properties of recycled concrete based on aggregate characteristics. *Science and Engineering of Composite Materials, 136(1)*, 516–527. https://doi.org/10.1515/secm-2021–0050

2. Thomas, C., de Brito, J., Cimentada, A., Sainz-Aja, J. A. (2022). Macro- and micro- properties of multi-recycled aggregate concrete. *Journal of Cleaner Production, 245,* 118843. https://doi.org/10.1016/j.jclepro.2019.118843

3. Wang, C., Xiao, J., Zhang, C., Xiao, X. (2020). Structural health monitoring and performance analysis of a 12-story recycled aggregate concrete structure. *Engineering Structures, 205,* 110102. https://doi.org/10.1016/j.engstruct.2019.110102

4. Xiao, J. Z., Hao, L. C., Cao, W. Z., Ye, T. H. (2022). Influence of recycled powder derived from waste concrete on mechanical and thermal properties of foam concrete. *Journal of Building Engineering, 61,* 105203. https://doi.org/10.1016/j.jobe.2022.105203

5. Shi, L., Liu, J., Wang, Y., Chiu, A. (2021). Cleaner production progress in developing and transition countries. *Journal of Cleaner Production, 278,* 123763. https://doi.org/10.1016/j.jclepro.2020.123763

6. Chakrdhara, R. M. (2018). Properties of recycled aggregate and recycled aggregate concrete: Effect of parent concrete. *Asian Journal of Civil Engineering, 19(1),* 103–110. https://doi.org/10.3390/su12229399

7. Zhang, H. H., Xiao, J. Z., Tang, Y. X., Duan, Z. H., Poon, C. S. (2022). Long-term shrinkage and mechanical properties of fully recycled aggregate concrete: Testing and modelling. *Cement & Concrete Composites, 130*, 104527. https://doi.org/10.1016/j.cemconcomp.2022.104527

8. Xiao, J. Z., Tang, Y. X., Chen, H. N., Zhang, H. H., Xia, B. (2022). Effects of recycled aggregate combinations and recycled powder contents on fracture behavior of fully recycled aggregate concrete. *Journal of Cleaner Production, 366,* 132895. https://doi.org/10.1016/j.jclepro.2022.132895

9. Marie, I., Mujall, R. (2019). Effect of design properties of parent concrete on the morphological properties of recycled concrete aggregates. *Engineering Science and Technology, An International Journal, 22(1),* 334–345. https://doi.org/10.1016/j.jestch.2018.08.014

10. Ye, T. H., Xiao, J. Z., Zhao, W. J., Duan, Z. H., Xu, Y. F. (2022). Combined use of recycled concrete aggregate and glass cullet in mortar: Strength, alkali expansion and chemical compositions. *Journal of Building Engineering, 55,* 104721. https://doi.org/10.1016/j.jobe.2022.104721

11. Geng, Y., Wang, Q. H., Wang, Y. Y., Zhang, H. (2019). Influence of service time of recycled coarse aggregate on the mechanical properties of recycled aggregate concrete. *Materials and Structures, 52(5),* 1–16. https://doi.org/10.1617/s11527-019-1395-0

12. Reichenbach, S., Kromoser, B. (2021). State of practice of automation in precast concrete production. *Journal of Building Engineering, 43,* 102527. https://doi.org/10.1016/j.jobe.2021.102527

13. Yu, N., Chen, C., Mahkamov, K., Han, F. T., Zhao, C. et al. (2020). Selection of a phase change material and its thickness for application in walls of buildings for solar-assisted steam curing of precast concrete. *Renewable Energy, 150,* 808–820. https://doi.org/10.1016/j.renene.2019.12.130

14. Wang, X. Y., Du, Q., Lu, C., Li, J. T. (2020). Exploration in carbon emission reduction effect of low-carbon practices in prefabricated building supply chain. *Journal of Cleaner Production, 368,* 133153. https://doi.org/10.1016/j.jclepro.2022.133153

15. Han, F. H., Zhang, Z. Q. (2018). Hydration, mechanical properties and durability of high-strength concrete under different curing conditions. *Journal of Thermal Analysis and Calorimetry, 132(2),* 823–834. https://doi.org/10.1007/s10973-018-7007-3

16. Lou, B. X., Ma, F. H. (2022). Crack extension resistance of steam-cured concrete under different curing temperature conditions. *Theoretical and Applied Fracture Mechanics, 119,* 103331. https://doi.org/10.1016/j.tafmec.2022.103331

17. Ma, H. Q., Zhang, S. H., Feng, J. J. (2022). Early hydration properties and microstructure evolutions of MgO-activated slag materials at different curing temperatures. *Ceramics International, 48,* 17104–17115. https://doi.org/10.1016/j.ceramint.2022.02.266

18. Li, G., Yao, F., Liu, P., Yan, C. H. (2016). Long-term carbonation resistance of concrete under initial high-temperature curing. *Materials and Structures, 49(7),* 2799–2806. https://doi.org/10.1617/s11527-015-0686-3

19. Daneshvar, D., Deix, K., Robisson, A. (2021). Effect of casting and curing temperature on the interfacial bond strength of epoxy bonded concretes. *Construction and Building Materials, 307,* 124328. https://doi.org/10.1016/j.conbuildmat.2021.124328

20. Shumuye, E. D., Zhao, J., Wang, Z. (2021). Effect of the curing condition and high-temperature exposure on ground-granulated blast-furnace slag cement concrete. *International Journal of Concrete Structures and Materials, 15,* 15. https://doi.org/10.1186/s40069-020-00437-6

21. Xu, G. D., Tian, Q., Miao, J. X., Liu, J. P. (2017). Early-age hydration and mechanical properties of high volume slag and fly ash concrete at different curing temperatures. *Construction and Building Materials, 149,* 367–377. https://doi.org/10.1016/j.conbuildmat.2017.05.080

22. Shi, J. Y., Liu, B. J., Shen, S., Tan, J. X., Dai, J. D. et al. (2020). Effect of curing regime on long-term mechanical strength and transport properties of steam-cured concrete. *Construction and Building Materials, 255,* 119407. https://doi.org/10.1016/j.conbuildmat.2020.119407

23. Algourdin, N., Pliya, P., Beaucour, A. L., Noumowé, A., di Coste, D. (2022). Effect of fine and coarse recycled aggregates on high-temperature behaviour and residual properties of concrete. *Construction and Building Materials, 341,* 127847. https://doi.org/10.1016/j.conbuildmat.2022.127847

24. Chen, B. F., Guan, B., Lu, X. C., Tian, B., Li, Y. B. (2022). Thermal conductivity evolution of early-age concrete under variable curing temperature: Effect mechanism and prediction model. *Construction and Building Materials, 319,* 126078. https://doi.org/10.1016/j.conbuildmat.2021.126078

25. Du, T., Li, C. Y., Wang, X. N., Ma, L., Qu, F. L. et al. (2022). Effects of pipe diameter, curing age and exposure temperature on chloride diffusion of concrete with embedded PVC pipe. *Journal of Building Engineering, 57,* 104957. https://doi.org/10.1016/j.jobe.2022.104957

26. Erdem, T. K., Turanli, L., Erdogan, T. Y. (2003). Setting time: An important criterion to determine the length of the delay period before steam curing of concrete. *Cement and Concrete Research, 33(5),* 741–745. https://doi.org/10.1016/S0008-8846(02)01058-X

27. Kjellsen, K. O. (1996). Heat curing and post-heat curing regimes of high-performance concrete: Influence on microstructure and C-S-H composition. *Cement and Concrete Research, 26(2),* 295–307. https://doi.org/10.1016/0008-8846(95)00202-2

28. Sajedi, F. (2012). Effect of curing regime and temperature on the compressive strength of cement-slag mortars. *Construction and Building Materials, 36,* 549–556. https://doi.org/10.1016/j.conbuildmat.2012.06.036

29. Narmluk, M., Nawa, T. (2011). Effect of fly ash on the kinetics of portland cement hydration at different curing temperatures. *Cement and Concrete Research, 41(6),* 579–589. https://doi.org/10.1016/j.cemconres.2011.02.005

30. Wang, J. J., Xie, J. H., Wang, C. H., Zhao, J. B., Liu, F. et al. (2020). Study on the optimum initial curing condition for fly ash and GGBS based geopolymer recycled aggregate concrete. *Construction and Building Materials, 247,* 118540. https://doi.org/10.1016/j.conbuildmat.2020.118540

31. Liu, H., Zhu, X. D., Zhu, P. H., Chen, C. H., Wang, X. J. et al. (2022). Carbonation treatment to repair the damage of repeatedly recycled coarse aggregate from recycled concrete suffering from coupling action of high stress and freeze-thaw cycles. *Construction and Building Materials, 349,* 128688. https://doi.org/10.1016/j.conbuildmat.2022.128688

32. Zhu, X. Y., Chen, X. D., Bai, Y., Ning, Y. J., Zhang, W. (2022). Evaluation of fracture behavior of high-strength hydraulic concrete damaged by freeze-thaw cycle test. *Construction and Building Materials, 321,* 126346. https://doi.org/10.1016/j.conbuildmat.2022.126346

33. Deng, X. H., Gao, X. Y., Wang, R., Gao, M. X., Yan, X. X. et al. (2021). Investigation of microstructural damage in air-entrained recycled concrete under a freeze-thaw environment. *Construction and Building Materials, 268,* 121219. https://doi.org/10.1016/j.conbuildmat.2020.121219

34. Huda, S. B., Shahria Alam, M. (2015). Mechanical and freeze-thaw durability properties of recycled aggregate concrete made with recycled coarse aggregate. *Journal of Materials in Civil Engineering, 27(10).* https://doi.org/10.1061/(ASCE)MT.1943-5533.0001237

35. Liu, K., Yan, J., Hu, Q., Sun, Y., Zou, C. (2016). Effects of parent concrete and mixing method on the resistance to freezing and thawing of air-entrained recycled aggregate concrete. *Construction and Building Materials, 106,* 264–273. https://doi.org/10.1016/j.conbuildmat.2015.12.074

36. Xiao, Q. H., Cao, Z. Y., Guan, X., Li, Q., Liu, X. L. (2019). Damage to recycled concrete with different aggregate substitution rates from the coupled action of freeze-thaw cycles and sulfate attack. *Construction and Building Materials, 221,* 74–83. https://doi.org/10.1016/j.conbuildmat.2019.06.060

37. Wang, W. J., Wang, Y., Chen, Q., Liu, Y. Z., Zhang, Y. et al. (2022). Bond properties of basalt fiber reinforced polymer (BFRP) bars in recycled aggregate thermal insulation concrete under freeze–thaw cycles. *Construction and Building Materials, 329,* 127197. https://doi.org/10.1016/j.conbuildmat.2022.127197

38. Liu, Z. W., Chin, C. S., Xia, J. (2022). Novel method for enhancing freeze–thaw resistance of recycled coarse aggregate concrete via two-stage introduction of denitrifying bacteria. *Journal of Cleaner Production, 346,* 131159. https://doi.org/10.1016/j.jclepro.2022.131159

39. Xiao, Q. H., Li, Q., Cao, Z. Y., Tian, W. Y. (2019). The deterioration law of recycled concrete under the combined effects of freeze-thaw and sulfate attack. *Construction and Building Materials, 200,* 344–355. https://doi.org/10.1016/j.conbuildmat.2018.12.066

40. Wei, D., Zhu, P. H., Yan, X. C., Liu, H., Chen, C. H. et al. (2022). Potential evaluation of waste recycled aggregate concrete for structural concrete aggregate from freeze-thaw environment. *Construction and Building Materials, 321,* 126291. https://doi.org/10.1016/j.conbuildmat.2021.126291

41. Standardization Administration of China (2010). *GB/T 25177-2010-Recycled coarse aggregate for concrete.* Beijing, China: Standardization Administration of China.

42. China Architecture and Building Press (2009). *GB/T 50082-2009-Standard for test methods of long-term performance and durability of ordinary concrete.* Beijing China: China Architecture and Building Press.

43. Ling, B. Y., Cai, R. H. (1982). Determination of technical indicators for the durability of concrete and reinforced concrete in seaport engineering. *Water Transportation Engineering, 2,* 52–56.

44. Li, J. Y., Peng, X. P., Zheng, Z. G., Cao, J. G., Guan, Y. S. et al. (2000). Quantitative design of frost resistance of concrete. *Concrete, 12,* 61–65.

45. Standardization Administration of China (2011). *GB/T 14685-2011-Pebble and crushed stone for construction.* Beijing, China: Standardization Administration of China.

46. Cassagnabère, F., Mouret, M., Escadeillas, G. (2009). Early hydration of clinker–slag–metakaolin combination in steam curing conditions, relation with mechanical properties. *Cement and Concrete Research, 39(12),* 1164–1173. https://doi.org/10.1016/j.cemconres.2009.07.023

47. He, Z. M., Long, G. C., Xie, Y. J. (2012). Influence of subsequent curing on water sorptivity and pore structure of steam-cured concrete. *Central South University, 19(4),* 1155–1162. https://doi.org/10.1007/s11771-012-1122-2

48. Wang, R. J., Zhang, Q. J., Li, Y. (2022). Deterioration of concrete under the coupling effects of freeze–thaw cycles and other actions: A review. *Construction and Building Materials, 319,* 126045. https://doi.org/10.1016/j.conbuildmat.2021.126045

49. China Architecture and Building Press (2019). *GB/T 50476-2019-Standard for design of concrete structure durability.* Beijing. China: Standardization Administration of China.

50. Wang, R. J., Hu, Z. Y., Li, Y., Wang, K., Zhang, H. (2022). Review on the deterioration and approaches to enhance the durability of concrete in the freeze–thaw environment. *Construction and Building Materials, 321,* 126371. https://doi.org/10.1016/j.conbuildmat.2022.126371

51. Kim, S. S., Qudoos, A., Jakhrani, S. H., Lee, J. B., Kim, H. G. (2019). Influence of coarse aggregates and silica fume on the mechanical properties, durability, and microstructure of concrete. *Materials, 12(20),* 3324–3337. https://doi.org/10.3390/ma12203324

52. Kjellsen, K. O., Detwiler, R. J. (1992). Reaction kinetics of portland cement mortars hydrated at different temperatures. *Cement and Concrete Research, 22(1),* 112–120. https://doi.org/10.1016/0008-8846(92)90141-H

53. Lu, B., Drissi, S., Liu, J. H., Hu, X., Song, B. X. et al. (2022). Effect of temperature on CO_2 curing, compressive strength and microstructure of cement paste. *Cement and Concrete Research, 157,* 106827. https://doi.org/10.1016/j.cemconres.2022.106827

54. Emmanuel, A. C., Krishnan, S., Bishnoi, S. (2022). Influence of curing temperature on hydration and microstructural development of ordinary portland cement. *Construction and Building Materials, 329,* 127070. https://doi.org/10.1016/j.conbuildmat.2022.127070

55. Snellings, R., Machner, A., Bolte, G., Kamyab, H., Durdzinski, P. et al. (2022). Hydration kinetics of ternary slag-limestone cements: Impact of water to binder ratio and curing temperature. *Cement and Concrete Research, 151,* 106647. https://doi.org/10.1016/j.cemconres.2021.106647

56. Yongjae, K., Asad, H., Muhammad, U., Wonjun, P. (2019). Influence of bonded mortar of recycled concrete aggregates on interfacial characteristics–porosity assessment based on pore segmentation from backscattered electron image analysis. *Construction and Building Materials, 212,* 149–163. https://doi.org/10.1016/j.conbuildmat.2019.03.265